



PAPER

Suppressing epidemic spreading in multiplex networks with social-support

OPEN ACCESS

RECEIVED

6 August 2017

REVISED

6 November 2017

ACCEPTED FOR PUBLICATION

23 November 2017

PUBLISHED

5 January 2018

Original content from this work may be used under the terms of the [Creative Commons Attribution 3.0 licence](#).

Any further distribution of this work must maintain attribution to the author(s) and the title of the work, journal citation and DOI.

Xiaolong Chen^{1,2}, Ruijie Wang^{1,3}, Ming Tang^{1,2,4}, Shimin Cai^{1,2}, H Eugene Stanley⁶ and Lidia A Braunstein^{5,6}¹ Web Sciences Center, University of Electronic Science and Technology of China, Chengdu 611731, People's Republic of China² Institute of Fundamental and Frontier Science & Big Data Research Center, University of Electronic Science and Technology of China, Chengdu 610054, People's Republic of China³ A Ba Teachers University, A Ba 623002, People's Republic of China⁴ School of Information Science Technology, East China Normal University, Shanghai 200241, People's Republic of China⁵ Instituto de Investigaciones Físicas de Mar del Plata (IFIMAR)-Departamento de Física, Facultad de Ciencias Exactas y Naturales, Universidad Nacional de Mar del Plata-CONICET, Funes 3350, (7600) Mar del Plata, Argentina⁶ Center for Polymer Studies and Department of Physics, Boston University, Boston, MA 02215, United States of AmericaE-mail: tangminghuang521@hotmail.com and shimin.cai81@gmail.com**Keywords:** multiplex networks, disease spreading, resources, phase transition

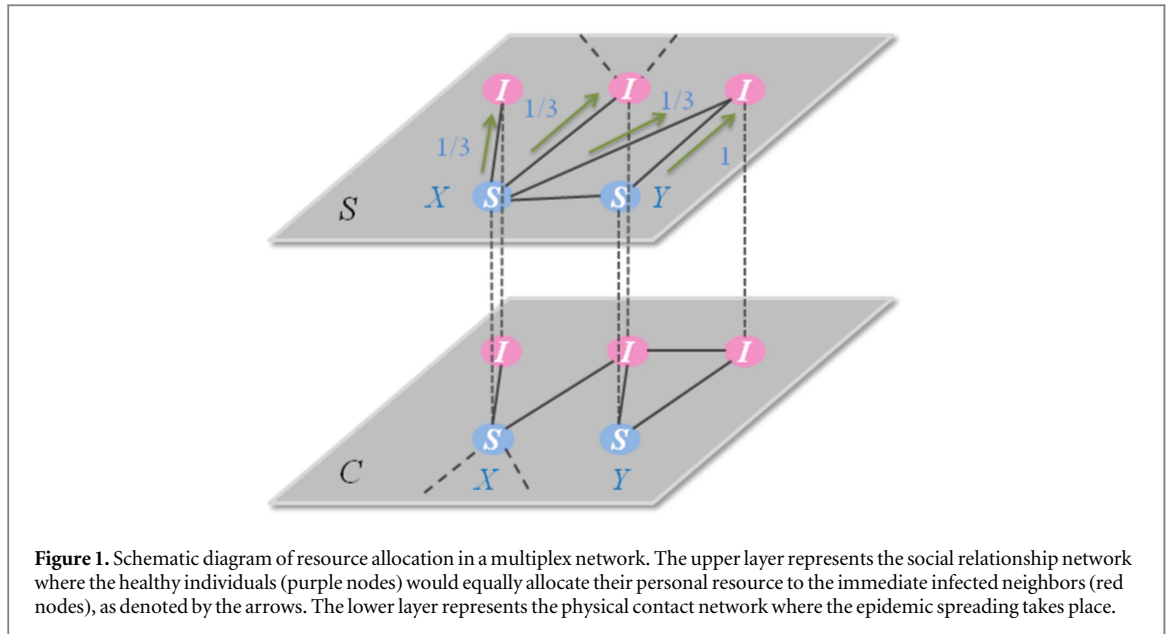
Abstract

Although suppressing the spread of a disease is usually achieved by investing in public resources, in the real world only a small percentage of the population have access to government assistance when there is an outbreak, and most must rely on resources from family or friends. We study the dynamics of disease spreading in social-contact multiplex networks when the recovery of infected nodes depends on resources from healthy neighbors in the social layer. We investigate how degree heterogeneity affects the spreading dynamics. Using theoretical analysis and simulations we find that degree heterogeneity promotes disease spreading. The phase transition of the infected density is hybrid and increases smoothly from zero to a finite small value at the first invasion threshold and then suddenly jumps at the second invasion threshold. We also find a hysteresis loop in the transition of the infected density. We further investigate how an overlap in the edges between two layers affects the spreading dynamics. We find that when the amount of overlap is smaller than a critical value the phase transition is hybrid and there is a hysteresis loop, otherwise the phase transition is continuous and the hysteresis loop vanishes. In addition, the edge overlap allows an epidemic outbreak when the transmission rate is below the first invasion threshold, but suppresses any explosive transition when the transmission rate is above the first invasion threshold.

1. Introduction

An outbreak of such diseases as SARS [1] and H5N1 [2, 3] puts at risk the lives of countless people. During the first nine months of the recent Ebola epidemic there were 4507 confirmed or probable cases of infection and 2296 deaths [4]. Increasing the investment of public resources to control a disease pandemic can be a serious economic burden, especially in developing countries [5, 6]. Many researches have been done on how to optimize scarce public health care and immunization resources when attempting to control an epidemic [7–10], the goal being to minimize the number of infected individuals by determining that optimal allocation [11].

A complex network science approach is now being widely used to determine the impact of resource investment on spreading dynamics. Böttcher *et al* [12] studied the impact of resource constraints on epidemic outbreaks and found that when the resources generated by the healthy population cannot cover the costs of healing the infected population the epidemics go out of control and discontinuous transitions [13–17] occur. Chen *et al* [18] explored the critical influence of resource expenditure on constraining epidemic spreading in networks and found that public resources can affect the stability of the disease outbreak. At a certain disease transmission rate there is a critical resource level above which a discontinuous phase transition in the infected population occurs. Böttcher *et al* [19] assumed that only the central nodes in a network can provide the necessary



care resource, and they found that a discontinuous transition in infected nodes occurs when the central nodes are surrounded by infected nodes. All of these researches focus on how public resource investment affects the spread of disease.

In real-world scenarios only a small percentage of patients are assisted by public resources. The majority depend on help from family and friends who provide economic [20–22] and emotional support [23, 24]. We thus study how social support from family and friends affects the dynamics of disease spreading. In a social network, a node has different connections in different settings. We can thus regard friendship ties (virtual contacts) and co-worker ties (physical contacts) as two different network layers. Although economic and medical resources and sources of information usually propagate through social relationships, diseases usually propagate through physical contacts. Thus we use a multiplex network of two-layers [25–28] to study how resource allocation in the social layer affects the spreading dynamics in the contact layer.

We use the susceptible-infected-susceptible (SIS) model in a multiplex network of two-layers to mimic the coupling dynamics between disease spreading and resource support. The disease propagates through the layer of physical contacts, but infected nodes seek help from their neighbors through the layer of social relations. Infected nodes receive resources from healthy neighbors and do not generate resources. We analyze the process using a dynamic message passing (DMP) approach [29–32]. We examine how degree heterogeneity affects the dynamical process and find that the infected density in the steady state (ρ) increases continuously at the first epidemic threshold and then jumps suddenly at the second threshold. Hysteresis loops exist in the phase transition of the infected density, and the size of the hysteresis region and the value of the invasion threshold decrease with the degree heterogeneity. Examining how edge overlap between the two layers affects the dynamics of spreading we find that the overlap has a critical value. When the overlap is below the critical value, the infected density first increases continuously and then discontinuously with disease transmission rate, and there are hysteresis loops. When the overlap is above the critical value, the phase transition of ρ is continuous and there is no hysteresis loop. We also find that when the transmission rate is below the first invasion threshold the disease outbreaks more easily for a large edge overlap, but when the transmission rate is above the first invasion threshold the edge overlap suppresses the disease spreading and the second invasion threshold increases as the overlap increases.

2. Epidemic model with social-support

In a multiplex network of two-layers, each layer has N nodes and each node in the first layer has a counterpart in the second layer. Here the upper layer is the social relationship network (e.g., Facebook friends and family members) from which healthy nodes allocate resources to infected neighbors (see layer S in figure 1). The lower layer is the physical contact network through which the disease spreads (see layer C in figure 1). Variables A and B are the adjacency matrices of layer S and C with elements a_{ij} and b_{ij} . If nodes i and j are connected by one edge in layer S , $a_{ij} = 1$, otherwise $a_{ij} = 0$. The same is true in layer C . We denote by s_v the node state variable of node v , and if it is in the susceptible state $s_v = 0$, otherwise $s_v = 1$. We assume that each healthy individual has a certain resource level r per unit time, which for simplicity we set at $r = 1$. Resources are distributed equally to infected

neighbors. Figure 1 shows that node X distributes one resource unit to three infected neighbors in layer S , and that node Y distributes one resource unit to one infected neighbor. For the sake of analytical tractability, we assume that the total resources are not cumulative in the system, and if healthy nodes do not allocate their resources to neighbors they consume these resources themselves. In addition, infected nodes consume all of the received resources at the current time step, and each healthy individual generates a new one-unit resource at the next time step. Using this definition, the resources that node j gives to node i in layer S is

$$R_{j \rightarrow i} = \frac{1}{\sum_v a_{jv} s_v}. \quad (1)$$

Without resource support a node recovers spontaneously at a rate μ_0 [35], and for simplicity we assume $\mu_0 = 0$. The recovery rate of i at time t is

$$\mu_i(t) = \mu_r \frac{R_i(t)}{k_i^S}, \quad (2)$$

where $\mu_i(t) \equiv \mu(R_i(t))$, and $R_i(t)$ is the expected resources that node i receives from healthy neighbors. The μ_r value is the coefficient that represents the efficiency of resource support from neighbors, $\mu_r \in [0, 1]$, and k_i^S is the degree of i in layer S . The recovery rate of infected nodes is assumed to be positively related to the resource received from healthy neighbors in layer S . In real-world setting the cost of repairing a vital node in a complex system is much higher than the cost of repairing a common node. For example, because hub airports in airline networks play a vital role in connecting a large number of countries and regions, the repairing cost when they fail is much higher than that for lower-degree airports [33]. Similarly, the cost of repairing hub nodes in brain networks is much higher than the cost of repairing common nodes [34]. The same is true in epidemic spreading. Individuals exposed to viruses over a long period of time, e.g., medical staff members who are in constant contact with infected individuals, have large degrees in physical contact networks. Community leaders are also hub nodes in high-degree physical contact networks. In both cases the cost of curing these hub nodes being infected is much higher than other infected nodes in the contact networks. Thus we assume that the recovery rate of an infected node is negatively related to its degree.

We use the classical SIS model to investigate the spreading process in multiplex networks. Each individual can be either infected or susceptible. Susceptible individuals are healthy and are then infected by an infected neighbor at a rate β . Infected individuals recover at a rate $\mu_i(t)$, which is assumed to be independent of the availability of social resources in previous researches [36, 37].

3. Dynamic message-passing method

We use dynamic message-passing method to analyze the spreading dynamics. In this method a variable ‘message’ passes through the directed edges of the network and does not backtrack to the source node. Our message is $\theta_{j \rightarrow i}$, the probability that node j is infected by its neighbors other than i . In addition, $\rho_i(t)$ is the probability that node i is in the infected state at time t . The probability that an infected node i will connect to a healthy node j in layer S is $a_{ij}(1 - \theta_{j \rightarrow i}(t))$, and the expected number of infected neighbors of node j is $\sum_{\ell \neq i} a_{j\ell} \theta_{\ell \rightarrow j}(t) + 1$, where the plus one takes into account that node i is infected. Thus the resource $R_i(t)$ that node i receives from healthy neighbors is

$$R_i(t) = \sum_j a_{ij}(1 - \theta_{j \rightarrow i}(t)) \frac{1}{\sum_{\ell \neq i} a_{j\ell} \theta_{\ell \rightarrow j}(t) + 1}. \quad (3)$$

Using this definition, the discrete-time version of evolution of $\rho_i(t)$ [38] is

$$\rho_i(t + \Delta t) = (1 - \rho_i(t))(1 - q_i(t)) + (1 - \mu_i(t))\rho_i(t), \quad (4)$$

where Δt is the time increment, which we set at $\Delta t = 1$, and $q_i(t)$ is the probability that i is not infected by any neighbor in layer C , which is given by

$$q_i(t) = \prod_{j \in \mathcal{N}_i^C} (1 - \beta \theta_{j \rightarrow i}(t)), \quad (5)$$

where \mathcal{N}_i^C is the neighbor set of i in layer C . Note that to exclude any contribution of node i to the infection of j , we adopt $\theta_{j \rightarrow i}(t)$ instead of $\rho_j(t)$ in equation (5). Similarly, the discrete-time version of evolution of $\theta_{j \rightarrow i}(t)$ is

$$\theta_{j \rightarrow i}(t + 1) = (1 - \theta_{j \rightarrow i}(t))(1 - \phi_{j \rightarrow i}(t)) + (1 - \mu_j(t))\theta_{j \rightarrow i}(t). \quad (6)$$

Here $(1 - \phi_{j \rightarrow i}(t))$ is the probability that j is infected by at least one neighbor other than i . Thus $\phi_{j \rightarrow i}(t)$ is

$$\phi_{j \rightarrow i}(t) = \prod_{\ell \in \mathcal{N}_j^C \setminus i} (1 - \beta \theta_{\ell \rightarrow j}(t)). \quad (7)$$

Here $\mathcal{N}_j^C \setminus i$ is the neighbor set of j excluding i , and the fraction of infected nodes at time t is

$$\rho(t) = \frac{1}{N} \sum_{i=1}^N \rho_i(t), \quad (8)$$

where $\rho_i(\infty) \equiv \rho_i$ and $\mu_i(t) \equiv \mu_i$ at the steady state $t \rightarrow \infty$. Solving equations (4) and (6) at the stationary state

$$\rho_i = (1 - \rho_i)(1 - q_i) + (1 - \mu_i)\rho_i \quad (9)$$

and

$$\theta_{j \rightarrow i} = (1 - \theta_{j \rightarrow i})(1 - \phi_{j \rightarrow i}) + (1 - \mu_j)\theta_{j \rightarrow i}, \quad (10)$$

we obtain the phase diagram of the model. We use iteration to numerically compute the evolution of the state of network nodes.

Due to nonlinearities in equations (3)–(7) they do not have a closed analytic form, and this disallows obtaining the epidemic threshold β_c . If $\beta > \beta_c$, $\rho > 0$, otherwise $\rho = 0$ in the steady state. When $\beta \rightarrow \beta_c$, $\rho_i \rightarrow 0$, $\theta_{j \rightarrow i} \rightarrow 0$, and the number of infected neighbors of each healthy node in layer S is approximately zero in the thermodynamic limit, prior to reaching the epidemic threshold $(1 - \theta_{j \rightarrow i}) \rightarrow 1$. If we add these assumptions to equation (3) resource R_i becomes $R_i \rightarrow k_i^S$, we will obtain the recovery rate $\mu_i \rightarrow \mu_r$ in the steady state (see figures 4(a) and 7(a)).

To compute the threshold, we linearize equations (6) and (7) around $\theta_{j \rightarrow i} = 0$ and obtain

$$q_i \approx 1 - \beta \sum_{j=1}^N b_{ji} \theta_{j \rightarrow i} \quad (11)$$

and

$$\phi_{j \rightarrow i} \approx 1 - \beta \sum \mathbf{B}_{j \rightarrow i, l \rightarrow h} \theta_{l \rightarrow h}, \quad (12)$$

where \mathbf{B} is the non-backtracking matrix [39] of layer C and

$$\mathbf{B}_{j \rightarrow i, l \rightarrow h} = \delta_{jh}(1 - \delta_{il}), \quad (13)$$

where δ_{il} is a Dirac delta function. Inserting equation (12) into (10) and neglecting second-order terms we obtain

$$\sum (-\delta_{ij} \delta_{ih} \mu_r + \beta \mathbf{B}_{j \rightarrow i, l \rightarrow h}) \theta_{l \rightarrow h} = 0. \quad (14)$$

To solve equation (14) we define a $2E \times 2E$ matrix \mathbf{J} , where E is the number of edges and the elements of \mathbf{J} are

$$\mathbf{J}_{j \rightarrow i, l \rightarrow h} = -\delta_{ij} \delta_{ih} \mu_r + \beta \mathbf{B}_{j \rightarrow i, l \rightarrow h}. \quad (15)$$

The system enters a global epidemic region in which the epidemic grows exponentially when the largest eigenvalue of \mathbf{J} is greater than zero [31, 32, 37]. Thus we can obtain the epidemic threshold as

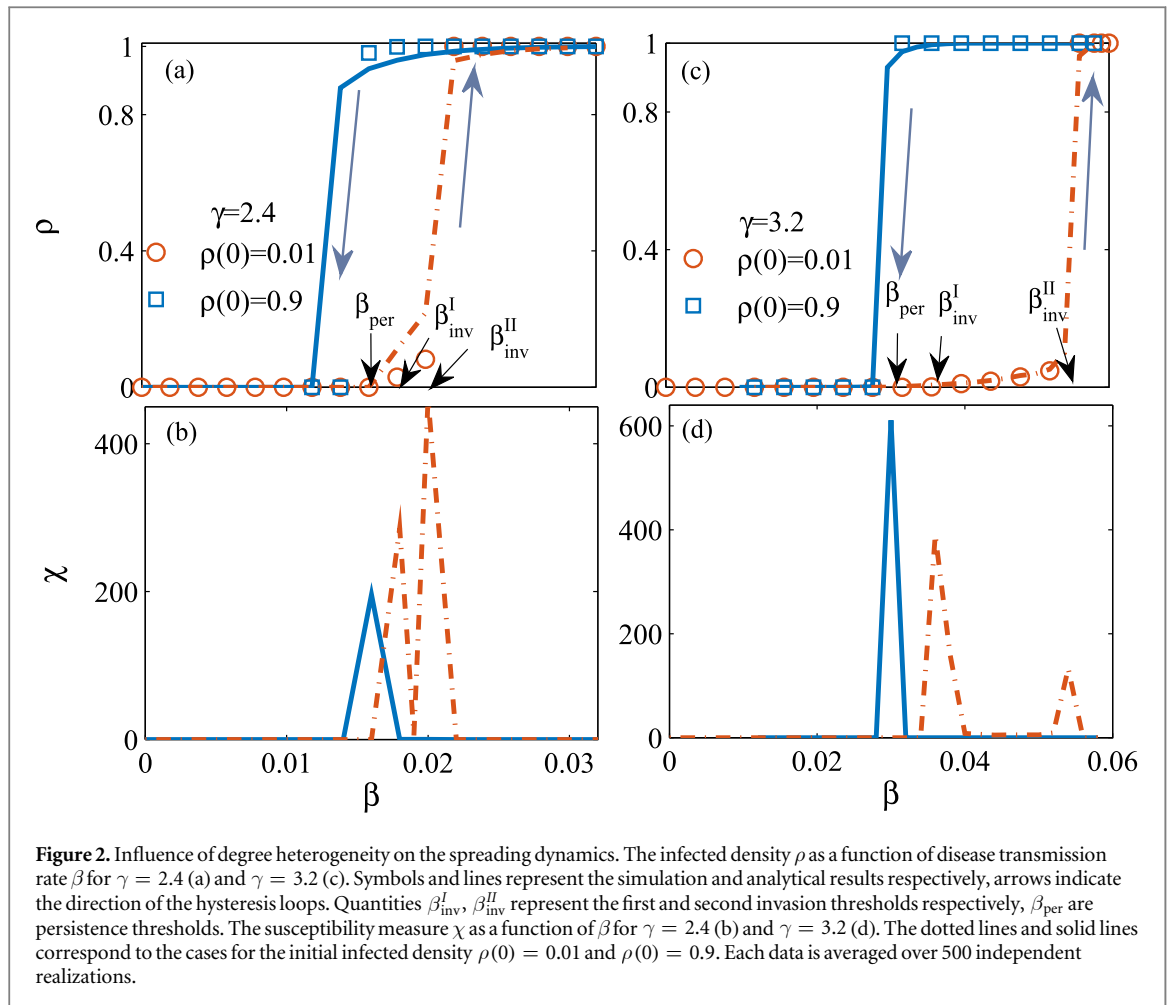
$$\beta_c = \frac{1}{\Lambda_J}, \quad (16)$$

where Λ_J is the largest eigenvalue of \mathbf{J} .

4. Numerical and simulation results

To examine how resource support affects epidemic dynamics, we perform numerical computations and stochastic simulations in the networks. Because many real-world complex networks have a highly skewed degree distribution, e.g., Facebook [40] and the World Wide Web [41], we focus on networks with a heterogeneous degree distribution. We assume that the two layers of the network have the same degree sequences ($k_i^S = k_i^C$). Thus for simplicity we denote k_i to be the degree of node i in both layers S and C .

To build our multiplex network we use an uncorrelated configuration model (UCM) [42] with a given degree distribution $P(k) \sim k^{-\gamma}$ in which γ is the degree exponent. Here a smaller γ implies a more heterogeneous degree distribution. The maximum degree is determined by the structural cut-off $k_{\max} \sim \sqrt{N}$ [43] and we set the minimum degree at $k_{\min} = 3$. In addition we disallow multiple and self-connections and set the network size as $N = 10000$. When studying resource support from neighbors, we eliminate any possibility of spontaneous recovery, i.e., $\mu_0 = 0$, and assume that node recovery is solely dependent on the amount of resources received. Here we set the efficiency parameter at $\mu_r = 0.6$ and the μ_r value does not affect the result [37, 44].



To determine the epidemic threshold, we use a susceptibility measure [45, 46]

$$\chi = N \frac{\langle \rho^2 \rangle - \langle \rho \rangle^2}{\langle \rho \rangle}, \quad (17)$$

where $\langle \dots \rangle$ is the ensemble averaging, and χ exhibits peaks at the transition points.

We now examine how degree heterogeneity and edge overlap between the two layers of the network affect its dynamic features.

4.1. Effects of degree heterogeneity

To investigate how degree heterogeneity affects spreading dynamics, we disallow any edge overlap between the two layers, i.e., nodes are randomly connected by edges in layer S and layer C , and the amount of edge overlap m_e is approximately 0 in the thermodynamic limit.

To examine ρ as a function of β , we randomly select one percent of the nodes to be seeds ($\rho(0) = 0.01$). Figures 2(a) and (b) show the epidemic spreading for $\gamma = 2.4$ and $\gamma = 3.2$. Note the hybrid phase transition in ρ that exhibits properties of both continuous and discontinuous phase transitions. As β increases ρ grows continuously at β_{inv}^I . Then an infinitely small increase in β induces a sudden jump of ρ at β_{inv}^I , where β_{inv}^I and β_{inv}^II are the first and second invasion thresholds. The ρ transition type indicates that there are three possible system states, (i) completely healthy, (ii) partially infected, and (iii) completely infected. This differs significantly from the classical SIS model. Note that when $\rho(0) = 0.9$, there is a discontinuous jump from 0 to 1 at β_{per} , which is in contrast to the case of $\rho(0) = 0.01$. In addition, we find hysteresis loops in the phase transition of ρ when $\gamma = 2.4$ and $\gamma = 3.2$ (see figures 2(a) and (c)). When the seed density is initially low, e.g., $\rho(0) = 0.01$, the disease breaks out at the invasion threshold β_{inv}^I , but when it is initially high, e.g., $\rho(0) = 0.9$, the disease breaks out at the persistence threshold β_{per} . The arrows in figures 2(a) and (b) indicate the direction of the hysteresis loops. We determine critical points β_{inv}^I and β_{inv}^II and persistence threshold β_{per} using the susceptibility χ shown in figures 2(b) and (d). The theoretical results obtained from the numerical iterations agree with the simulation results (see the lines in figures 2(a) and (b)).

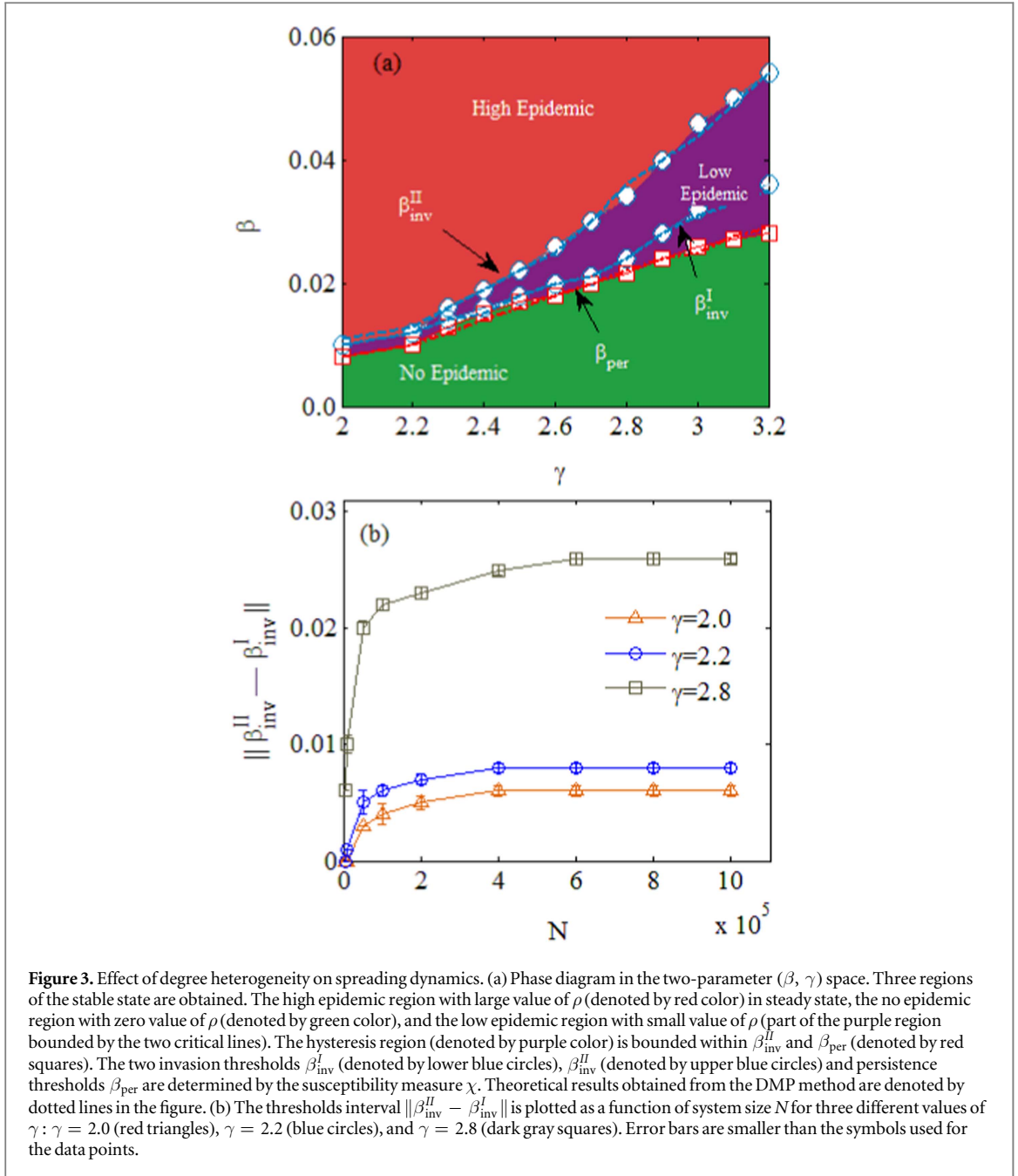


Figure 3. Effect of degree heterogeneity on spreading dynamics. (a) Phase diagram in the two-parameter (β, γ) space. Three regions of the stable state are obtained. The high epidemic region with large value of ρ (denoted by red color) in steady state, the no epidemic region with zero value of ρ (denoted by green color), and the low epidemic region with small value of ρ (part of the purple region bounded by the two critical lines). The hysteresis region (denoted by purple color) is bounded within β_{inv}^{II} and β_{per}^I (denoted by red squares). The two invasion thresholds β_{inv}^I (denoted by lower blue circles), β_{inv}^{II} (denoted by upper blue circles) and persistence thresholds β_{per}^I are determined by the susceptibility measure χ . Theoretical results obtained from the DMP method are denoted by dotted lines in the figure. (b) The thresholds interval $\|\beta_{inv}^{II} - \beta_{inv}^I\|$ is plotted as a function of system size N for three different values of γ : $\gamma = 2.0$ (red triangles), $\gamma = 2.2$ (blue circles), and $\gamma = 2.8$ (dark gray squares). Error bars are smaller than the symbols used for the data points.

We next determine how degree heterogeneity (i.e., parameter γ) influences the spreading dynamics. Figure 3(a) shows the two-parameter (β, γ) phase diagram. The parameter space is partitioned into three regions according to ρ value. When $\beta < \beta_{inv}^I$, the system falls into the no-epidemic regime, i.e., the green and part of the purple area below β_{inv}^I . When $\beta_{inv}^I \leq \beta < \beta_{inv}^{II}$, it falls into the low-epidemic regime (bounded by two critical lines) in which ρ increases slowly with β . Finally, above β_{inv}^{II} , ρ suddenly jumps to the high epidemic regime (red) in which approximately all nodes are infected. The regime between invasion threshold β_{inv}^I and persistence threshold β_{per}^I is the hysteresis region (purple). The values of β_{inv}^I and β_{inv}^{II} both increase with γ . Although we can obtain the theoretical value of β_{inv}^I from equation (16), we cannot obtain the theoretical value of β_{inv}^{II} and β_{per}^I by linearizing the equations around $\rho_i \rightarrow 0$ and $\theta_{j \rightarrow i} \rightarrow 0$ and thus we must apply numerical methods using equations (4) and (6). We first define a judgment value ϵ that is linear with system size N . Without loss of generality we set $\epsilon = 0.3$. We then define the jump size $\Delta\rho$ to be

$$\Delta\rho = \rho(\beta) - \rho(\beta - \Delta\beta), \quad (18)$$

where $\Delta\beta$ is an infinitesimal increment in β , which we set at $\Delta\beta = 0.001$, and $\rho(\beta)$ is the infected density in the steady state when the transmission rate is β . We obtain the threshold when $\Delta\rho \geq \epsilon$ is at a certain β value in the thermodynamic limit [16, 47]. Using the numerical method, we obtain the second invasion threshold β_{inv}^{II} and the persistence threshold β_{per}^I . Figure 3 shows that the theoretical values marked by dotted lines agree with the

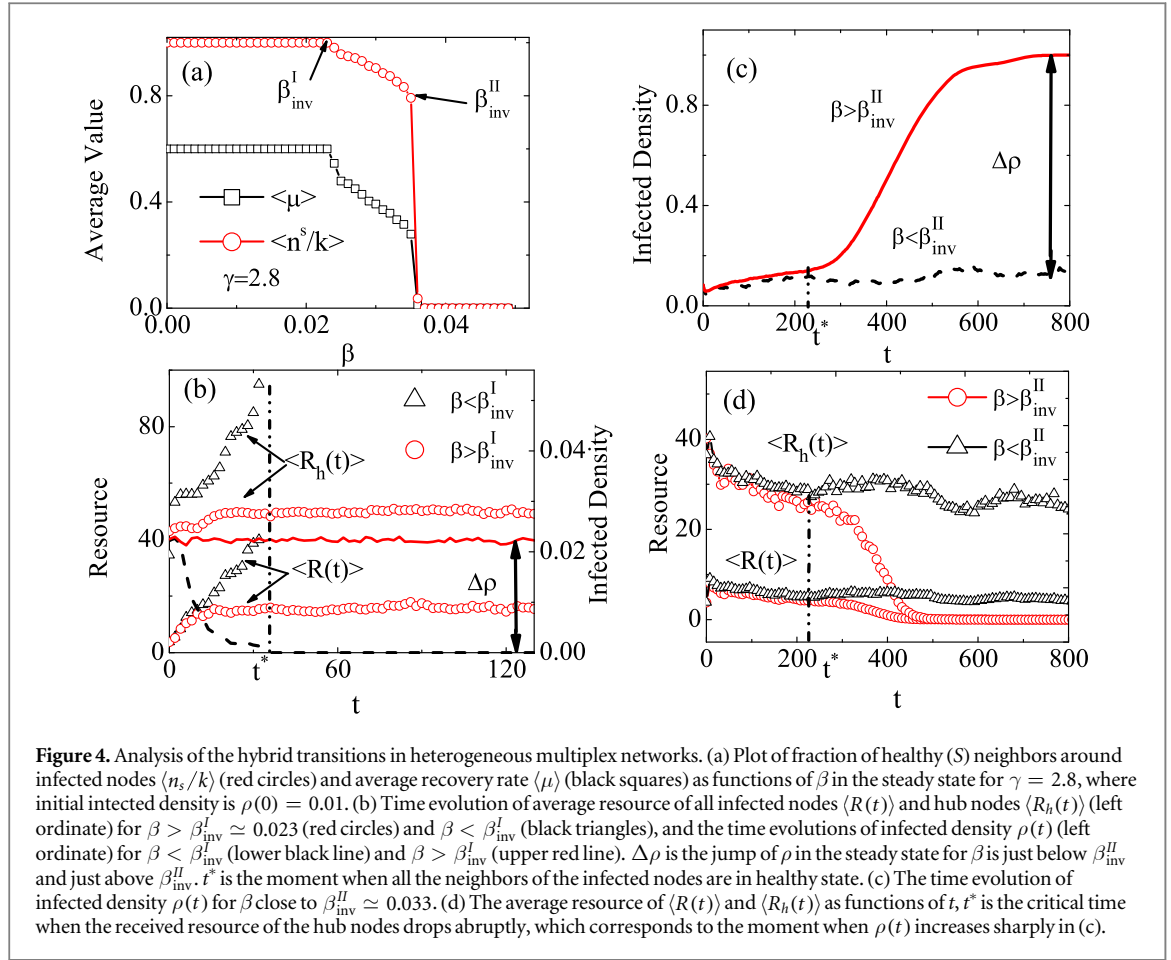


Figure 4. Analysis of the hybrid transitions in heterogeneous multiplex networks. (a) Plot of fraction of healthy (S) neighbors around infected nodes $\langle n_s/k \rangle$ (red circles) and average recovery rate $\langle \mu \rangle$ (black squares) as functions of β in the steady state for $\gamma = 2.8$, where initial infected density is $\rho(0) = 0.01$. (b) Time evolution of average resource of all infected nodes $\langle R(t) \rangle$ and hub nodes $\langle R_h(t) \rangle$ (left ordinate) for $\beta < \beta_{inv}^I \simeq 0.023$ (red circles) and $\beta > \beta_{inv}^I$ (black triangles), and the time evolutions of infected density $\rho(t)$ (left ordinate) for $\beta < \beta_{inv}^I$ (lower black line) and $\beta > \beta_{inv}^I$ (upper red line). $\Delta\rho$ is the jump of ρ in the steady state for β is just below β_{inv}^I and just above β_{inv}^I . t^* is the moment when all the neighbors of the infected nodes are in healthy state. (c) The time evolution of infected density $\rho(t)$ for β close to $\beta_{inv}^I \simeq 0.033$. (d) The average resource of $\langle R(t) \rangle$ and $\langle R_h(t) \rangle$ as functions of t , t^* is the critical time when the received resource of the hub nodes drops abruptly, which corresponds to the moment when $\rho(t)$ increases sharply in (c).

simulation results. The change in the system state among the three regions indicates that the phase transitions of ρ are hybrid. Figure 3(a) shows that the low epidemic and hysteresis regions expand as γ increases.

To demonstrate that there are two invasion thresholds in networks with heterogeneous degree distribution, we use a finite-size scaling analysis [48]. Figure 3(b) shows the interval in $\beta_{inv}^I \leq \beta < \beta_{inv}^II$, which we denote $\|\beta_{inv}^II - \beta_{inv}^I\|$, as a function of N for $\gamma = 2.0$, $\gamma = 2.2$, and $\gamma = 2.8$, where $\|\cdot\|$ is the norm operator. Figure 3(b) shows the values of $\|\beta_{inv}^II - \beta_{inv}^I\|$ converging asymptotically to positive constant values in the thermodynamic limit, i.e., $\lim_{N \rightarrow \infty} \|\beta_{inv}^II - \beta_{inv}^I\| \simeq 0.006$ for $\gamma = 2.0$, $\lim_{N \rightarrow \infty} \|\beta_{inv}^II - \beta_{inv}^I\| \simeq 0.008$ for $\gamma = 2.2$, and $\lim_{N \rightarrow \infty} \|\beta_{inv}^II - \beta_{inv}^I\| \simeq 0.026$ for $\gamma = 2.8$, which implies the two invasion thresholds do not merge when $\gamma \leq 2.2$ and the two are always present in networks with a heterogeneous degree distribution.

To analyze the sudden jump of ρ and the hysteresis loops, we examine the transmission process analytically using mean-field approximation in random regular networks (RRNs), which corresponds to the limit $\gamma \rightarrow \infty$. Through a bifurcation analysis we account for the existence of the sudden jump of ρ and the hysteresis loops (see appendix information). Note that the first threshold β_{inv}^I disappears in the RRNs and the transition of ρ is discontinuous when it is not hybrid (see figure A2(a)).

To explain the hybrid transition when γ is finite, i.e., when $\gamma \leq 3.2$, we investigate the number of susceptible neighbors around each infected node in layer S and their recovery rates as a function of β . In the steady state the number of each infected node's susceptible neighbors in layer S is n_s , and their fraction n_s/k_i . Here the recovery rate is μ_i . To evaluate the collective state, we examine the average quantity $\langle n_s/k \rangle$ of n_s/k_i and the average quantity $\langle \mu \rangle$ of the recovery rate. Figure 4(a) shows values of $\langle n_s/k \rangle$ and $\langle \mu \rangle$ as functions of β for $\gamma = 2.8$. We find that both $\langle n_s/k \rangle$ and $\langle \mu \rangle$ are constant when $\beta < \beta_{inv}^I$, which implies zero values for ρ . They then slowly decrease until they reach the β_{inv}^I , at which point an infinitesimal increase in β causes a jump in $\langle n_s/k \rangle$ and $\langle \mu \rangle$. Figures 4(b)–(d) show the time dependence near β_{inv}^I and β_{inv}^II . Figure 4(b) shows the time evolution of the infected density $\rho(t)$ around $\beta_{inv}^I \simeq 0.023$ for $\gamma = 2.8$. The difference in $\rho(\infty)$ for β just below and above threshold β_{inv}^I is $\Delta\rho$ (see equation (18)). Note that $\rho(\infty)$ increases slowly at β_{inv}^I , i.e., a small increment $\Delta\rho \simeq 0.022$. We next examine the time evolutions of the average resources of the infected nodes $\langle R(t) \rangle$ and the hub nodes $\langle R_h(t) \rangle$. Note that without loss of generality we can assign hub node status to nodes with a degree larger than $k = 30$. Note also that when β is just below β_{inv}^I both $\langle R(t) \rangle$ and $\langle R_h(t) \rangle$ increase until $t = t^*$, which implies that all infected nodes have acquired sufficient resources to recover and $\rho(t)$ evolves to zero. In contrast,

when β is just above β_{inv}^I , as the promotion effect of the hub nodes, the disease will spread on a finite scale centered by these nodes. The processes of infection and recovery take place repeatedly among these nodes when $t \rightarrow t_\infty$. Thus infection and recovery processes are balanced, and the values of $\langle R(t) \rangle$ and $\langle R_h(t) \rangle$ fluctuate around a finite value when $t \rightarrow t_\infty$ (see figure 4(b)). As β smoothly increases at $\beta = \beta_{\text{inv}}^I$, the level of available resources decreases continuously as the number of infected nodes increases (see figures 4(a)). Thus the density of infection increases continuously at β_{inv}^I . Figures 4(c) and (d) show a critical time $t^* \simeq 220$ at which β is approximately $\beta_{\text{inv}}^{II} \simeq 0.033$. At the early stage of the propagation process, i.e., when $t < t^*$, the disease spreads through the local seed nodes. Because most of neighbors of the infected nodes in layer S remain healthy, they have a sufficient resource level to recover. Here the infection and recovery processes are balanced. As the $\rho(t)$ value increases slowly the available resources levels $\langle R_h(t) \rangle$ and $\langle R(t) \rangle$ for $\beta \simeq \beta_{\text{inv}}^{II}$ slowly decrease (see figures 4(c) and (d)). When $\beta < \beta_{\text{inv}}^{II}$ the infection and recovery processes remain balanced when $t \rightarrow \infty$, thus the density of infection fluctuates around a small finite value when $t \rightarrow t_\infty$ ($\rho(\infty) \simeq 0.18$) (see figure 4(c)). Note that as hub nodes disappear in the RRNs the disease is suppressed until β reaches a threshold at which point it jumps discontinuously, the balance disappears (see appendix), and only one threshold remains. When $\beta > \beta_{\text{inv}}^{II}$ the transmission rate is relatively large and the balance between infection and recovery is broken. Infecting the healthy nodes in layer C decreases the resources available to the nodes in layer S and delays the recovery of infected nodes. This recovery delay increases the effective transmission probability in layer C , more healthy nodes are infected, and both the available resources and the recovery rate decrease. This causes a cascading infection in system nodes that is accelerated when hub nodes are surrounded by infected nodes, and this can cause total system failure. Figure 4(d) shows an abrupt drop of $\langle R_h(t) \rangle$ and $\langle R(t) \rangle$ at t^* when $\beta > \beta_{\text{inv}}^{II}$. Figure 4(c) shows a rapid increase in the density of infection from a small value $\rho(t^*) \simeq 0.18$ to a high value $\rho(\infty) \simeq 1.0$. Note that in the steady state the large difference $\Delta\rho$ between $\beta < \beta_{\text{inv}}^{II}$ and $\beta > \beta_{\text{inv}}^{II}$ causes explosive transitions. This explains the hybrid transition in networks with a heterogeneous degree distribution.

At last, we give a qualitative explanation to the jump of ρ from 0 to 1 with $\rho(0) = 0.9$. When $\beta < \beta_{\text{per}}$, there is a small transmission rate. Thus only a small amount of resources ($\rho(0)$ is large) can provide a relatively large recovery rate. Then the basic reproduction number is less than 1, and more infected nodes get recovery as time goes on. Consequently, a larger amount of resources will be generated and the recovery rate is further improved. Thus, when $t \rightarrow t_\infty$, $\rho(t)$ decreases to 0 gradually. However, when $\beta \geq \beta_{\text{per}}$, there is a larger transmission rate, and the limit initial resources of the healthy nodes can not meet the recovery of a large number of nodes. As time goes on, the recovery rate of infected decreases with the reduction of resources gradually. The recovery delay enhances the effective transmission rate, and resources further decrease. Then a cascading process forms and at last the disease evolves rapidly to the entire network ($\rho = 1.0$). Thus when the initial fraction of infected nodes is large, i.e., $\rho(0) = 0.9$, ρ jumps from 0 to 1, which is in contrast to the case of $\rho(0) = 0.01$.

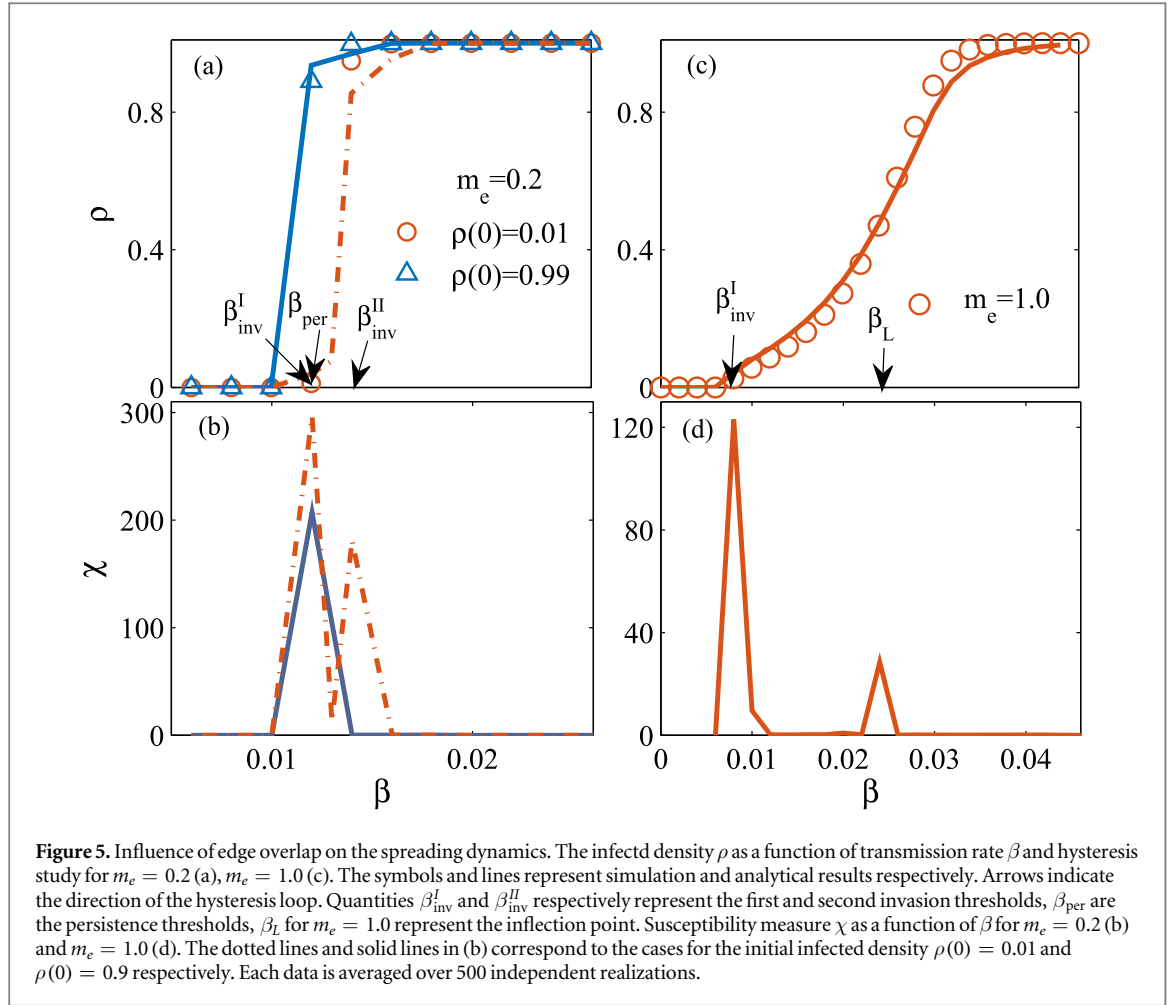
Figure 4(d) shows the evolution of the resource level in the hub nodes. This explains the decrease in the two invasion thresholds and the gap that appears between the two thresholds with the increase of degree heterogeneity. A more heterogeneous network has more hub nodes and is more sensitive to increases in β . Thus increasing the degree heterogeneity reduces the gap between the two thresholds (see figure 3).

These numerical and simulation results differ greatly from the classical SIS model. In the multiplex networks with a heterogeneous degree distribution, degree heterogeneity enhances disease spreading and the phase transition is hybrid. Besides, there are hysteresis loops in the phase transition of ρ , and the interval between the two invasion thresholds and the hysteresis region decreases as degree heterogeneity increases. When $\gamma \rightarrow \infty$ the network is approximately a RRN, β_{inv}^I disappears as hub nodes disappear, and the transition is discontinuous.

4.2. Effects of edge overlap

In social networks two individuals can be friends in the social relation layer and coworkers in the physical contact layer. In transportation networks two cities can be connected by both an expressway and a railway. Thus edge overlap is essential in the science of complex networks, especially when studying percolation in multiplex networks [49]. Here we examine how the amount of edge overlap m_e between the two layers affects the spreading dynamics. To eliminate the effect of structure, we fix the values $\gamma = 2.2$ and $\langle k \rangle = 9$. We then use UCM to build a multiplex network with two identical layers $m_e = 1.0$. To generate a variety of m_e values, with a probability $q = 1 - m_e$ we rewire pairs of links in layer S .

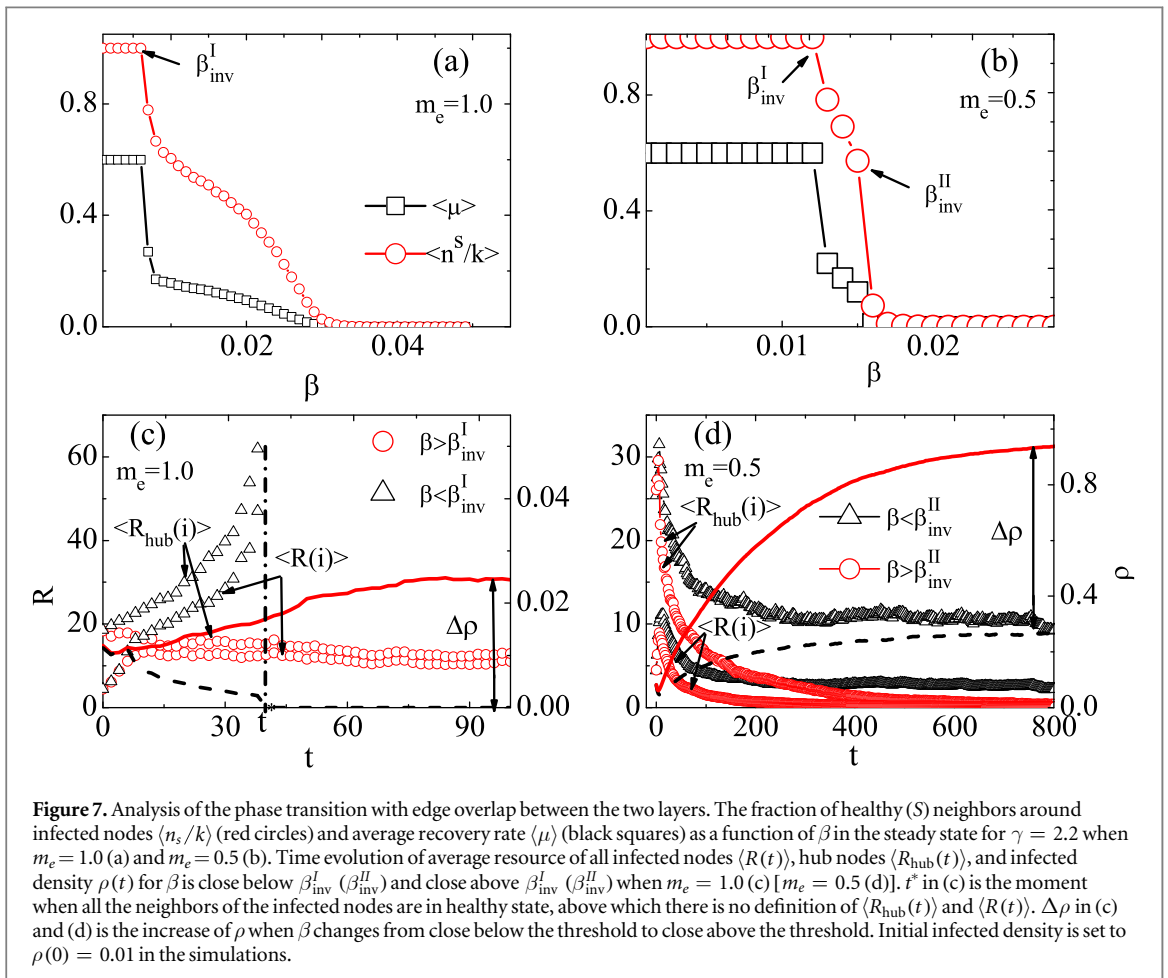
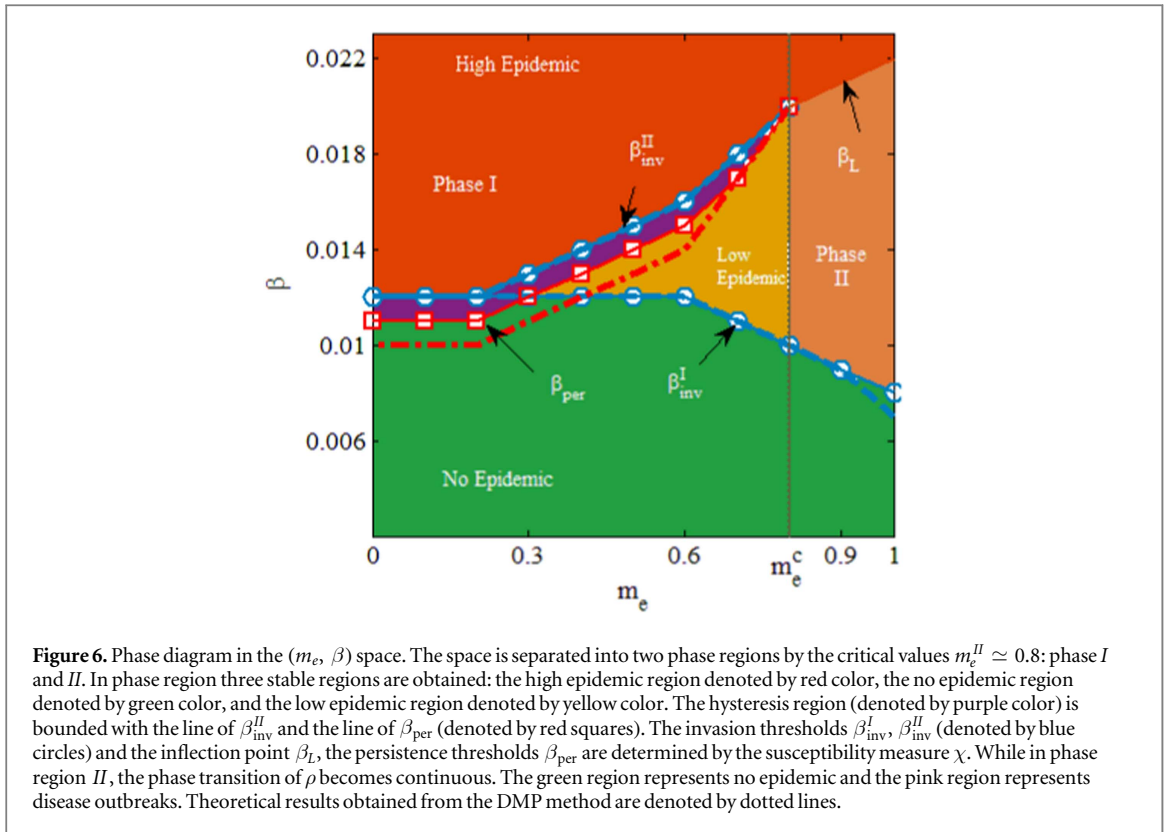
Figures 5(a) and (c) show the infected density ρ as a function of β with two typical values $m_e = 0.2$ (a) and $m_e = 1.0$ (c). Note that when the edges between the two layers overlap completely ($m_e = 1.0$) the infected density ρ smoothly increases from 0 to 1 and there is no hysteresis loop (see figure 5(c)). When the rate of edge overlap between two layers is lowered, i.e., when $m_e = 0.2$, a hybrid phase transition appears (see figure 5(a)). The infected density ρ smoothly increases at $\beta = \beta_{\text{inv}}^I$ and then the system acquires a low epidemic region ($\beta_{\text{inv}}^I < \beta < \beta_{\text{inv}}^{II}$) in which ρ slowly increases. Subsequently at $\beta = \beta_{\text{inv}}^{II}$ an infinitesimally small increase in β causes an abrupt jump in ρ and the disease suddenly spreads throughout the entire system. Hysteresis loops appear in the transition process and the arrows indicate their direction. Figures 5(b) and (d) show that the



invasion thresholds (i.e., β_{inv}^I) and β_{inv}^{II} and the persistence threshold β_{per} are determined by the susceptibility χ . Note that the hysteresis loop disappears when $m_e = 1.0$ (see figure 5(c)), and it no longer satisfies the definition of $\epsilon > 0.3$ at β_L . Thus β_L is an inflection point at which the increase in ρ accelerates. The theoretical results from the DMP method agree with the simulation results.

To determine how the amount of edge overlap between the two layers affects the spreading dynamics, we perform simulations for values of m_e from 0 to 1 and obtain the space in the plane (β, m_e) shown in figure 6. The parameter space is separated into phase regions I and II by a critical value of edge overlap $m_e^c \simeq 0.8$. When $m_e < m_e^c$ the system falls into phase I in which the phase transition of ρ is hybrid and the space is again separated into three regions by two invasion thresholds β_{inv}^I (lower blue circles) and β_{inv}^{II} (upper blue circles). When $\beta < \beta_{inv}^I$ the system has a no-epidemic region (green) in which all nodes are healthy and in a steady state. When $\beta_{inv}^I \leq \beta < \beta_{inv}^{II}$ the system has a low-epidemic region (orange) in which the infected density ρ increases continuously from 0 to a finite value until it reaches the second invasion threshold β_{inv}^{II} . Figure 3(b) shows a small low-epidemic region when $m_e \leq 0.2$ such that when $\gamma = 2.2$ and $m_e = 0.0$ the value of $\|\beta_{inv}^{II} - \beta_{inv}^I\|$ converges to a non-zero constant value when $N \rightarrow \infty$. When $\beta \geq \beta_{inv}^{II}$ the system jumps abruptly to a high epidemic region (red) in which the disease spreads throughout the entire system. The hysteresis loops (purple) appear in phase I. In contrast, when $m_e \geq m_e^c$ the system falls into phase II in which the phase transition of ρ is continuous. The value of ρ smoothly increases from 0 to 1 and the hysteresis loops disappear. Figure 6 shows that when $\beta < \beta_{inv}^I$ the value of β_{inv}^I decreases as the amount of edge overlap increases. Here edge overlap promotes disease spreading. When $\beta \geq \beta_{inv}^I$ the value of β_{inv}^{II} increases as the amount of edge overlap increases. Here edge overlap suppresses disease spreading. We obtain the theoretical value of β_{inv}^I using equation (16) and β_{inv}^{II} and β_{per} using the method in section 4.1. Figure 6 shows that the theoretical values marked by the dotted lines agree with simulation results.

To clarify these results, figures 7(a) and (b) show a plot of the average recovery rate $\langle \mu \rangle$ and the number of susceptible neighbors around each infected individual $\langle n_s/k \rangle$ as functions of β . Note that when the two layers overlap completely ($m_e = 1.0$), $\langle n_s/k \rangle$ and $\langle \mu \rangle$ decrease at the first threshold β_{inv}^I to a certain value and then decrease continuously to zero, indicating that the infected density in the steady state increases continuously up



to 1 as β increases. In contrast, when $m_e = 0.5$ there are two abrupt jumps of $\langle n_s/k \rangle$ and $\langle \mu \rangle$ at β_{inv}^I and β_{inv}^H , respectively. Here $\langle \mu \rangle$ jumps sharply to zero at β_{inv}^H (see figure 7(b)) indicating an explosive jump in ρ .

Figures 7(c) and (d) show the time dependence of the infected density and the resource value. Figure 7(c) shows the average resource of all infected nodes $\langle R(t) \rangle$ and the average resource of hub nodes $\langle R_h(t) \rangle$ as a function of t for $m_e = 1.0$. Note that when β is immediately below β_{inv}^I both $\langle R_h(t) \rangle$ and $\langle R(t) \rangle$ increase continuously until $t = t^*$. When $t > t^*$ there is no definition of resource because all infected nodes recover (see $\rho(t)$ for $\beta < \beta_{\text{inv}}^I$ at $t = t^*$). When $\beta \geq \beta_{\text{inv}}^I$ the infection and recovery rates are balanced, and both $\langle R_h(t) \rangle$ and $\langle R(t) \rangle$ fluctuate around a finite value when $t \rightarrow t_\infty$. Thus all the infected nodes recover with a certain probability and $\rho(t)$ also fluctuates around a finite value when $t \rightarrow t_\infty$ (see $\rho(t)$ for $\beta > \beta_{\text{inv}}^I$). With an increase in β , resource availability decreases continuously as the number infected nodes increases until the disease spreads throughout the system and no available resources remain (see figures 7(a) and (c)). This accounts for the continuous increase in ρ when $m_e = 1.0$.

Figure 7(d) shows the time evolution of the infected density and available resource level for $m_e = 0.5$. Note that when β is immediately below β_{inv}^H at the early stage the disease propagates within the local range of seed nodes, and there are sufficient healthy neighbors in layer S to temporarily suppress the spread. This causes a brief increase in available resources at the beginning of the propagation process and a slight decline in the density of infection. Subsequently the disease rapidly spreads along the edges in layer C. When edges in layer S link out ($m_e = 0.5$), with a high probability that infected nodes in layer S infect their neighbors, $\langle R_h(t) \rangle$ and $\langle R(t) \rangle$ rapidly decline, and $\rho(t)$ rapidly increases. Eventually infection and recovery become balanced, and $\rho(t)$, $\langle R_h(t) \rangle$, and $\langle R(t) \rangle$ converge to finite values. When $\beta > \beta_{\text{inv}}^H$ there is also a temporary increase in both the available resources and the density of infection. However, when the propagation begins, unlike when $m_e = 1.0$ (see figures 4(c) and (d)) there is no balanced period at the beginning of the process. The infection of the S-state nodes reduces the resource available to a large number of infected nodes in layer S and delays their recovery. This recovery delay further increases the transmission probability in layer C. Thus $\langle R_h(t) \rangle$ and $\langle R(t) \rangle$ decline sharply to zero, the density of infection rapidly increases to 1, and cascading infection occurs.

An increase in the overlap between two layers indicates an increase in the local social circle of an individual. When an individual's colleagues (those frequently in contact, defined as the contact layer) and friends (the social relations, defined as the social layer) are the same group of people, the links in these two layers largely overlap. When $\beta < \beta_{\text{inv}}^I$, seed nodes initially transmit the disease only to immediate neighbors with whom they are in frequent contact. This high-value local effect causes infected nodes to have a higher probability of linking with other infected nodes in layer S and lowers the level of resources available from neighbors. Thus the overlap between two layers increases network fragility against the invasion of the disease, and increases the probability of an epidemic breakout, and thus lowers the epidemic threshold β_{inv}^I . In contrast, a lower value of overlap rate between the two layers indicates a more global social circle, neighbors of nodes in the social layer differ from neighbors in the contact layer. The infected nodes in the contact layer can acquire resources from healthy neighbors in the social layer. Thus the network is more robust against the invasion of the disease, and there is a relatively high epidemic threshold β_{inv}^I . This is the reason β_{inv}^I decreases as m_e increases, as shown in figure 6. When $\beta_{\text{inv}}^I \leq \beta < \beta_{\text{inv}}^H$, hub nodes promote disease transmission, the disease breaks out in a finite range, a sufficient number of healthy neighbors are present in layer S to help infected nodes to recover, and infection and recovery remain balanced. Figure 7(d) shows that the value of resource availability fluctuates around a finite value when $t \rightarrow t_\infty$, and the density of infection converges continuously to a finite value ($\rho \simeq 0.28$). Thus in this region the global connections in a social layer have an advantage over the local connections (see figures 5 (a) and (c)). When $\beta \geq \beta_{\text{inv}}^H$ the disease breaks out rapidly and globally, and the balance between infection and recovery is broken. When $m_e < m_e^c$ (a relatively low overlap rate), the connections in layer S are more global. The infection of a small number of S-state nodes in layer C influences the recovery of a large number of I-state nodes in layer S. Thus there is a delay in the recovery of infected nodes that further increases the transmission probability, promotes the disease spreading in layer C, and causes global cascading failure. This explains the increase in β_{inv}^H with m_e and the explosive jump of ρ (see figure 7(c)) when $m_e < m_e^c$. In contrast, when $m_e > m_e^c$, the connections of layer S is more localized, and the infection of nodes in layer C delays the recovery of the infected nodes within only a small range in layer S. This small range in recovery delay does not globally increase the effective transmission probability. Thus as the effective transmission probability gradually increases the value of ρ smoothly increases with β (see figures 7(a) and (c)).

5. Conclusions

We have investigated how the level of social support affects spreading dynamics using the SIS model in social-contact coupled networks. Links in the social layer represent relationships between friends or families through which healthy nodes allocate recovery resources to infected neighbors. Links in the contact layer represent daily

physical contacts through which the disease can spread. Infected nodes do not have resources, and their recovery depends on obtaining resources in layer S from healthy neighbors. We assume the recovery rate of an infected node to be a function of the resources received from healthy neighbors. We use the DMP method to analyze the spreading dynamics. We first examine how degree heterogeneity impacts disease spreading. We find that degree heterogeneity enhances disease spreading, and due to the existence of hub nodes there is a balanced interval $\beta_{\text{inv}}^I < \beta < \beta_{\text{inv}}^{II}$ in which the infection and recovery processes remain balanced. The value of ρ increases continuously from 0 to a finite value at the first invasion threshold β_{inv}^I , increases slowly in $\beta_{\text{inv}}^I < \beta < \beta_{\text{inv}}^{II}$, then suddenly jumps at β_{inv}^{II} . Thus the transition of ρ is hybrid. In addition, increasing the degree exponent γ in the network increases the gap between the two thresholds and the hysteresis region. To analyze the sudden jump of ρ and the hysteresis loops, we examine the spreading process analytically using mean-field approximation in RRNs. Through a bifurcation analysis we account for the existence of the sudden jump of ρ and the hysteresis loops. In addition, in the RRNs the balanced interval disappears when there is a lack of hub nodes. The first invasion threshold β_{inv}^I thus disappears.

We next fix the degree heterogeneity and investigate the effect of edge overlap between the two layers. We find that there is a critical value m_e^c . When $m_e < m_e^c$ there is a second invasion threshold β_{inv}^{II} that increases with m_e . The value of ρ smoothly increases at β_{inv}^I and then suddenly jumps at β_{inv}^{II} , revealing the transition of ρ to be hybrid with the presence of hysteresis loops in this region (see figure 6). In contrast, when $m_e > m_e^c$ the phase transition of ρ is continuous and the hysteresis loops disappear. In addition, when $\beta < \beta_{\text{inv}}^I$ seed nodes can only transmit the disease locally at the early stage. Here an increase in global connectivity with a lower rate of overlap in the social layer (layer S) increases the probability of linking to healthy neighbors and increases the probability that infected nodes will recover. Thus the first invasion threshold β_{inv}^I decreases as the overlap rate m_e increases. When $\beta > \beta_{\text{inv}}^I$, increasing the transmission rate increases the fraction of infected nodes, and an increase in global connectivity in layer S increases the probability of linking to infected neighbors and lowers the recovery rate. Thus the second invasion threshold β_{inv}^{II} increases with m_e when $m_e < m_e^c$.

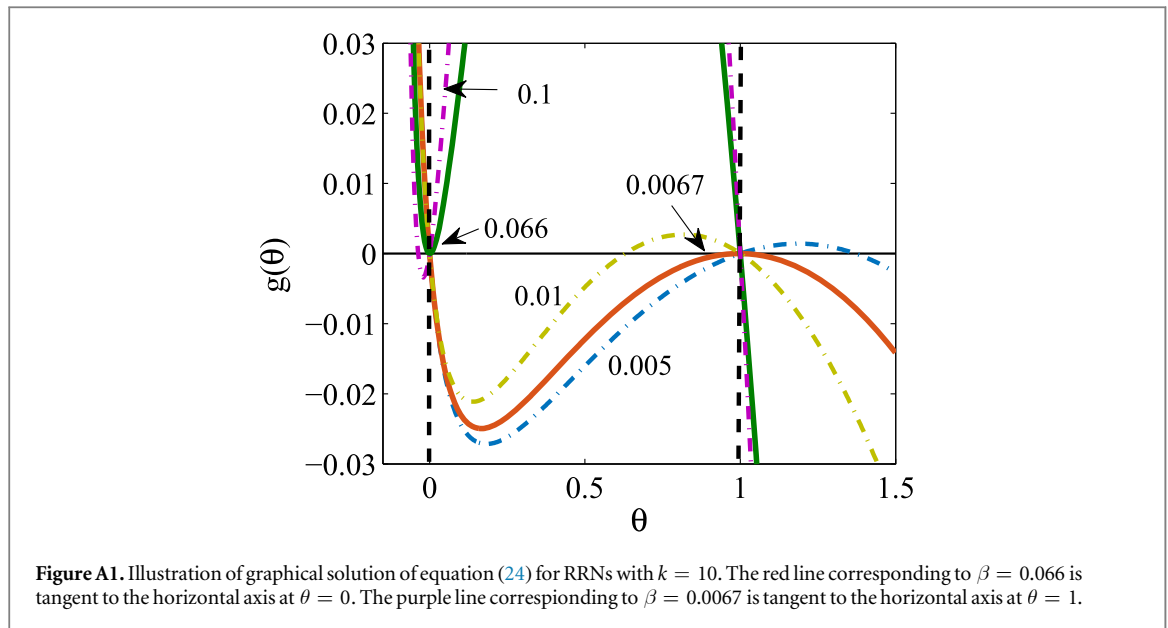
Although researchers in different scientific fields have focused on ways of constraining disease epidemics in human populations, most scientific literatures have been devoted to questions concerning the optimum allocation of public resources or the impact of government investment on spreading dynamics. There has been little examination of how social supports affect spreading dynamics, and our novel model fills this gap. Whereas, there are still some limits of our model. For example, for the sake of analytical tractability, we assume that the resources of each node in layer S are not cumulative. This kind of phenomenon has certain rationality in the real world. For example, the healthy individuals will generate a certain amount of resources in their daily life. To maintain their lives, resources will also be consumed. Basically, the generation and consumption of resources remain balance during a period, and there will not be many resources to accumulate for most individuals. Thus, we make the assumption that the resources generated in current step will be consumed out. Although the assumption is reasonable to a certain extent, a more prevalent phenomenon is that resources such as economic wealth and human resources are cumulative over time. It will be interesting to consider the following questions. (a) How it would affect the dynamics of disease spreading if resources are accumulative over time? (b) Is the accumulation of resources an efficient way to prevent epidemic outbreaks or is just delaying the infection? Moreover, in real world, the Matthew effect [51] such as the the phenomenon that the rich tend to get richer is ubiquitous. Thus it will be interesting to consider the effect of preference-driven resource allocation on spreading dynamics. These are some open questions and possible directions after this work that will definitely motivate future works.

Acknowledgments

This work was supported by the National Natural Science Foundation of China under Grant Nos. 11575041 and 61673086, the Fundamental Research Funds for the Central Universities under Grant No. ZYGX2015J153. LAB is supported by UNMDP and Agencia, Pict 0429/2013. The Boston University Center for Polymer Studies is supported by NSFGrants PHY-1505000, CMMI-1125290 and CHE-1213217, by DTRA GrantHDTRA1-14-1-0017 and by DOE Contract DE-AC07-051d14517.

Appendix

When $\gamma \rightarrow \infty$ the system is approximately a RRN. To analyze the hysteresis loop and the sudden jump of ρ , we solve equations (4) and (6) analytically for RRN using mean-field approximation. In the mean-field approximation for a RRN, the degree of each node has the same value and the same probability of being infected. Because we have only considered the case $k_i^S = k_i^C$, for simplicity we denote the degree to be k . Each edge in the network also has the same probability of connecting with infected neighbors. Thus we define $\rho(t)$ and $\theta(t)$ such



that $\rho(t) = \rho_i(t) = \rho_j(t)$ and $\theta(t) = \theta_{j \rightarrow i}(t) = \theta_{i \rightarrow h}(t)$. Consequently the resource that each infected node can receive from healthy neighbors is

$$R(t) = \frac{k(1 - \theta(t))}{(k - 1)\theta(t) + 1} \tag{19}$$

and the recovery rate of each node is

$$\mu(t) = \frac{\mu_r(1 - \theta(t))}{(k - 1)\theta(t) + 1}. \tag{20}$$

When we approximate $1 - (1 - \beta\theta(t))^k$ as $k\beta\theta(t)$ and $1 - (1 - \beta\theta(t))^{(k-1)}$ as $(k - 1)\beta\theta(t)$ for small β we obtain

$$\frac{d\rho(t)}{dt} = k\beta\theta(t)(1 - \rho(t)) - \frac{\mu_r(1 - \theta(t))}{(k - 1)\theta(t) + 1}\rho(t) \tag{21}$$

and

$$\frac{d\theta(t)}{dt} = \beta(k - 1)\theta(t)(1 - \theta(t)) - \frac{\mu_r(1 - \theta(t))}{(k - 1)\theta(t) + 1}\theta(t). \tag{22}$$

The steady state of the spreading process corresponds to conditions $d\rho(t)/dt = 0$ and $d\theta(t)/dt = 0$. We denote $\theta(\infty)$ as θ and obtain

$$\theta(1 - \theta) \left[\beta(k - 1) - \frac{\mu_r}{(k - 1)\theta + 1} \right] = 0. \tag{23}$$

We also define $g(\theta)$ as the function of θ in the steady state, which is

$$g(\theta) = \theta(1 - \theta) \left[\beta(k - 1) - \frac{\mu_r}{(k - 1)\theta + 1} \right]. \tag{24}$$

Here $g(\theta)$ is tangent to the horizontal axis at $\theta_c(\infty)$, which is the critical value in the limit $t \rightarrow \infty$. The critical condition is

$$\left. \frac{dg(\theta)}{d\theta} \right|_{\theta_c} = 0. \tag{25}$$

Solving equation (25) we also obtain the critical transmission rate.

In order to analyze clearly the bifurcation phenomenon in RRNs, we give an example that illustrates the relationship between ρ and β when $k = 10$ in figure A1. We can observe that the number of solutions for equation (24) is dependent on β . Besides, $g(\theta)$ is tangent to the horizontal axis at $\theta = 1.0$ and $\theta = 0.0$ when $\beta \simeq 0.0067$ and $\beta \simeq 0.066$ respectively, which implies the existence of two critical values of β . From the whole parameter space of θ , we can observe that the transcritical bifurcations [50] occur at $\beta \simeq 0.0067$ and $\beta \simeq 0.066$ respectively. Specifically, there are three solutions (one unstable and two stable) passing to two solutions (one stable and one saddle point) and then, passing to three solutions (two stable and one unstable that goes into the

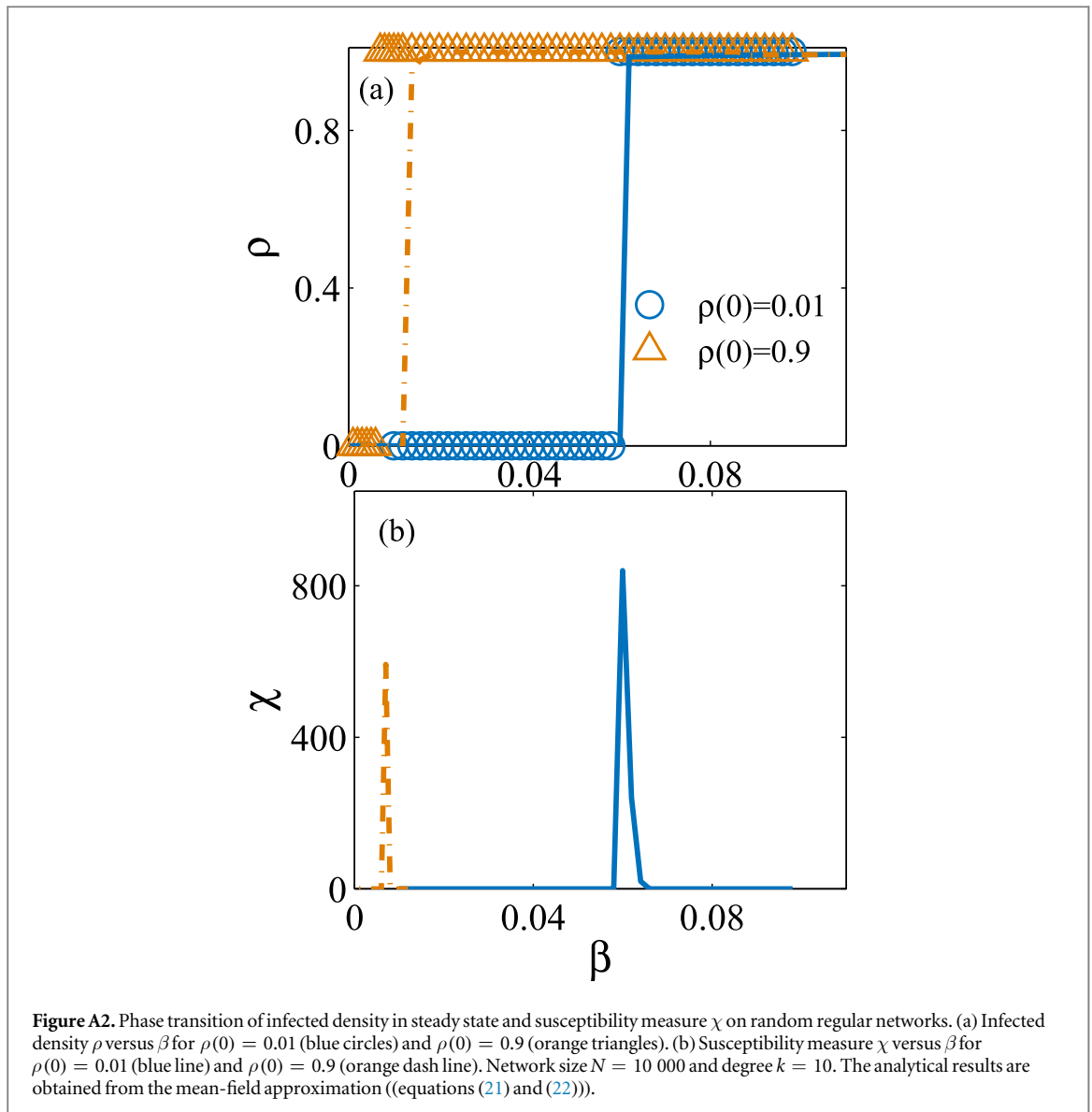


Figure A2. Phase transition of infected density in steady state and susceptibility measure χ on random regular networks. (a) Infected density ρ versus β for $\rho(0) = 0.01$ (blue circles) and $\rho(0) = 0.9$ (orange triangles). (b) Susceptibility measure χ versus β for $\rho(0) = 0.01$ (blue line) and $\rho(0) = 0.9$ (orange dash line). Network size $N = 10\,000$ and degree $k = 10$. The analytical results are obtained from the mean-field approximation (equations (21) and (22)).

unit interval of values of θ) at $\beta \simeq 0.0067$. The same transcritical bifurcations occur at $\beta \simeq 0.066$. However, the above conclusions are only mathematically significant. Physically, the value of θ can only locate in the interval of $[0, 1]$, as shown in the region between the two vertical dotted line at $\theta = 1.0$ and $\theta = 0.0$. The stable solutions at $\theta > 1.0$ and $\theta < 0.0$ have no physical meaning. Thus in fact, in the region $\theta \in [0, 1]$, equation (24) passes from two solutions (one stable and one unstable) in $\beta \in [0, 0.0067]$ to three solutions (one unstable that goes into the the unit interval of values of θ , and two stable) in $\beta \in (0.0067, 0.066)$ and then, to two solutions (one stable and one unstable). From bifurcation analysis above we can learn that the physically meaningful stable solution of θ will suddenly increase, and there is an alternate outcome—explosive growth in ρ . Whether the unstable state stabilizes to an outbreak state ($\theta > 0, \rho > 0$) or an extinct state ($\theta = 0, \rho = 0$) depends on the initial infection density $\rho(0)$, thus a hysteresis loop emerges. To distinguish the two thresholds of the hysteresis loop, we denote β_{per} as the persistence threshold corresponding to the solution $\theta_c > 0$ ($\theta_c = 1.0$ in RRNs) of equation (24) at which the disease initially has a large $\rho(0)$ value. Here β_{inv} is the invasion threshold corresponding to the nontrivial solution $\theta_c = 0$ of equation (24) at which the disease initially has a small $\rho(0)$ value. The interval $[\beta_{\text{per}}, \beta_{\text{inv}})$ is the hysteresis region.

Figure A2(a) shows the numerical and simulation results in RRNs with a degree $k = 10$. In RRNs the first invasion threshold β_{inv}^1 disappears and the transition of ρ is discontinuous, i.e., not hybrid. Since in RRNs, all nodes approximately have the same infection and recovery rate as they have almost the same amount of infected neighbors in physical contact layer and the same amount of healthy neighbors in social-relation layer. Thus when $\beta < \beta_{\text{inv}}$, there are sufficient resources to guarantee the recovery of the infected nodes, i.e., $\rho(t) \rightarrow 0$ when $t \rightarrow t_\infty$. However, when $\beta \geq \beta_{\text{inv}}$, there is a larger transmission rate among the pairs of infected and susceptible nodes, and resources that each infected nodes can get from healthy neighbors decreases, which

induces reduction of the recovery rate for all nodes. The recovery delay of the infected nodes in turn enhances the effective transmission rate and the infection range. Then, the available resources further diminish and a cascade process forms, thus the disease evolves rapidly to the entire network. Therefore, there are only two potential states of the system, namely all the infection or all the healthy, which is in contrast to the case of network with heterogeneity degree distribution. In a network with heterogeneity degree distribution, nodes have different infection and recovery probabilities. At each time step, nodes with larger degrees have larger infection probabilities, which promotes the spreading of disease. Thus, when β is around β_{inv}^I , as the promotion effect of hub nodes, the disease will spread on finite scales centered by these hub nodes, as shown in figure 4(b). In addition, we can observe from figure A2(a) that the hysteresis loops exist in the transition of ρ . The orange dashed line and the blue line correspond to the theoretical results for $\rho(0) = 0.01$ and $\rho(0) = 0.9$, respectively, obtained from equations (21) and (22). Figure A2(b) shows the susceptibility measurement χ versus β for $\rho(0) = 0.01$ and $\rho(0) = 0.9$. From these results we find that the theoretical results obtained from the mean-field approximation agree with the simulation results in RRNs.

References

- [1] Meyers L A, Pourbohloul B, Newman M E, Skowronski D M and Brunham R C 2005 *J. Theor. Biol.* **232** 71
- [2] Yuen K et al 1998 *Lancet* **351** 467
- [3] de Jong M D et al 2006 *Nat. Med.* **12** 1203
- [4] Team W E R 2014 *New Engl. J. Med.* **2014** 1481
- [5] Gallup J L and Sachs J D 2001 *Am. J. Trop. Med. Hyg.* **64** 85
- [6] Kirigia J M, Sambo L G, Yokouide A, Soumbeay-Alley E, Muthuri L K and Kirigia D G 2009 *BMC Int. Health Human Rights* **9** 8
- [7] Stinnett A A and Paltiel A D 1996 *J. Health Econ.* **15** 641
- [8] Wang L Y, Haddix A C, Teutsch S M and Caldwell B 1999 *Am. J. Manage. Care* **5** 445
- [9] Zaric G S and Brandeau M L 2002 *Math. Med. Biol.* **19** 235
- [10] Brandeau M L 2005 *Operations Research and Health Care* (Berlin: Springer)
- [11] Brandeau M L, Zaric G S and Richter A 2003 *J. Health Econ.* **22** 575
- [12] Böttcher L, Woolley-Meza O, Araújo N A, Herrmann H J and Helbing D 2015 *Sci. Rep.* **5** 16571
- [13] Araújo N A and Herrmann H J 2010 *Phys. Rev. Lett.* **105** 035701
- [14] Nagler J, Tiessen T and Gutch H W 2012 *Phys. Rev. X* **2** 031009
- [15] DSouza R M and Nagler J 2015 *Nat. Phys.* **11** 531
- [16] Chen X L, Yang C, Zhong L F and Tang M 2016 *Chaos* **26** 083114
- [17] Boccaletti S et al 2016 *Phys. Rep.* **660** 1
- [18] Chen X L, Zhou T, Feng L, Yang C, Wang M M, Fan X M and Hu Y Q 2016 arXiv:1611.00212
- [19] Böttcher L, Woolley-Meza O, Goles E, Helbing D and Herrmann H 2016 *Phys. Rev. E* **93** 042315
- [20] Seeman T E 1996 *Ann. Epidemiol.* **6** 442
- [21] Schulz R and Sherwood P R 2008 *J. Soc. Work Educ.* **44** 105
- [22] Drummond M F, Sculpher M J, Claxton K, Stoddart G L and Torrance G W 2015 *Methods for the Economic Evaluation of Health Care Programmes* (Oxford: Oxford University Press)
- [23] Cohen S E and Syme S 1985 *Social Support and Health* (San Diego, CA: Academic Press)
- [24] Thoits P A 1995 *J. Health Soc. Behav.* **2** 5379
- [25] Gomez S, Diaz-Guilera A, Gomez-Gardenes J, Perez-Vicente C J, Moreno Y and Arenas A 2013 *Phys. Rev. Lett.* **110** 028701
- [26] Granell C, Gomez S and Arenas A 2013 *Phys. Rev. Lett.* **111** 128701
- [27] Bianconi G and Radicchi F 2016 arXiv:1610.08708
- [28] De Domenico M, Granell C, Porter M A and Arenas A 2016 *Nat. Phys.* **12** 901906
- [29] Karrer B and Newman M E 2010 *Phys. Rev. E* **82** 016101
- [30] Shrestha M and Moore C 2014 *Phys. Rev. E* **89** 022805
- [31] Shrestha M, Scarpino S V and Moore C 2015 *Phys. Rev. E* **92** 022821
- [32] Wang W, Tang M, Stanley H E and Braunstein L A 2017 *Rep. Prog. Phys.* **80** 036603
- [33] Guimera R, Mossa S, Turtschi A and Amaral L N 2005 *Proc. Natl Acad. Sci. USA* **102** 7794
- [34] Bullmore E and Sporns O 2012 *Nat. Rev. Neurosci.* **13** 336
- [35] Valdez L D, Di Muro M A and Braunstein L A 2016 *J. Stat. Mech.* **E093402**
- [36] Pastor-Satorras R and Vespignani A 2001 *Phys. Rev. Lett.* **86** 3200
- [37] Pastor-Satorras R, Castellano C, Van Mieghem P and Vespignani A 2015 *Rev. Mod. Phys.* **87** 925
- [38] Gomez S, Arenas A, Borge-Holthoefer J, Meloni S and Moreno Y 2010 *Europhys. Lett.* **89** 38009
- [39] Krzakala F, Moore C, Mossel E, Neeman J, Sly A, Zdeborova L and Zhang P 2013 *Proc. Natl Acad. Sci. USA* **110** 20935
- [40] Viswanath B, Mislove A, Cha M and Gummadi K P 2009 *Proc. 2nd ACM Workshop on Online Social Networks* pp 37–42
- [41] Adamic L A and Huberman B A 2000 *Science* **287** 2115
- [42] Catanzaro M, Boguñá M and Pastor-Satorras R 2005 *Phys. Rev. E* **71** 027103
- [43] Boguna M, Pastor-Satorras R and Vespignani A 2004 *Euro. Phys. J. B* **38** 205
- [44] Pastor-Satorras R and Vespignani A 2001 *Phys. Rev. Lett.* **86** 3200
- [45] Ferreira S C, Castellano C and Pastor-Satorras R 2012 *Phys. Rev. E* **86** 041125
- [46] Shu P, Wang W, Tang M, Zhao P and Zhang Y C 2016 *Chaos* **26** 063108
- [47] Nagler J, Levina A and Timme M 2011 *Nat. Phys.* **7** 265
- [48] Newman M and Barkema G 1999 *Monte Carlo Methods in Statistical Physics* (Oxford: Oxford University Press)
- [49] Cellai D, Lopez E, Zhou J, Gleeson J P and Bianconi G 2013 *Phys. Rev. E* **88** 052811
- [50] Strogatz S 1994 *Nonlinear Dynamics and Chaos: With Applications* (Reading, MA: Addison-Wesley)
- [51] Perc M 2014 *J. R. Soc. Interface* **11** 20140378